NeuroImage 329 (2026) 121821

Contents lists available at ScienceDirect

NeuroImage

journal homepage: www.elsevier.com/locate/ynimg

Longitudinal comparison of adaptive neuroplasticity in two rat models of unilateral vestibulopathy by dual-tracer [^{18}F]FDG and [^{18}F]UCB-H PET

Isabelle S. Fuxjäger [a], Melissa Antons [a,b], Emna Marouane [c,d], Giulia Leschiutta [a], Rosel Oos [e], Giovanna Palumbo [e], Dilara Steenken [a], Simon Lindner [e], Sibylle Ziegler [e,f], Peter Bartenstein [e], Matthias Brendel [e,g,h], Rudolf Werner [e], Andreas Zwergal [a,i,*]

[a] German Center for Vertigo and Balance Disorders (DSGZ), LMU University Hospital, LMU Munich, Munich, Germany
[b] Department of Radiology, LMU University Hospital, LMU Munich, Munich, Germany
[c] Aix Marseille Université-CNRS, Laboratoire de Neurosciences Cognitives, LNC UMR 7291, Marseille, Groupe de Recherche Vertige (GDR#2074), France
[d] Normandie Université, UNICAEN, INSERM, COMETE, CYCERON, CHU Caen, 14000, Caen, France
[e] Department of Nuclear Medicine, LMU University Hospital, LMU Munich, Munich, Germany
[f] Clinic for Nuclear Medicine, Hannover Medical School (MHH), Hannover, Germany
[g] German Center for Neurodegenerative Diseases (DZNE), Munich, Germany
[h] Munich Cluster for Systems Neurology (SyNergy), Munich, Germany
[i] Department of Neurology, LMU University Hospital, LMU Munich, Munich, Germany

ARTICLE INFO

Keywords:
Unilateral vestibular neurectomy
Unilateral chemical labyrinthectomy
Acute unilateral vestibulopathy
Vertigo
Dizziness
Neuroimaging
Synaptic density
Animal models

ABSTRACT

Animal models of acute unilateral vestibulopathy are well established for the study of adaptive lesion-induced neuroplasticity, because symptoms of acute vestibular asymmetry such as nystagmus and postural imbalance recover over time as central vestibular compensation mechanisms commence action. The purpose of this study was to compare these mechanisms in a postganglionic complete unilateral vestibular neurectomy model (UVN) vs. a preganglionic incomplete chemical unilateral labyrinthectomy model (cUL) using a longitudinal [^{18}F]FDG/[^{18}F]UCB-H dual tracer positron emission tomography (PET) approach accompanied by multimodal behavioral testing. Twenty-four male Sprague Dawley rats underwent either cUL or UVN. Postoperatively, [^{18}F]FDG PETs were conducted weekly for four weeks to depict changes of [^{18}F]FDG as a surrogate for functional plasticity, and [^{18}F]UCB-H PETs were carried out at three time points over nine weeks to visualize alterations in synaptic density indicating structural plasticity. Behavioral recovery was assessed weekly using a clinical scoring system and open field evaluation. Behavioral data reflected comparable compensation dynamics between groups. Both [^{18}F]FDG and [^{18}F]UCB-H PET revealed a similar spatial pattern of brain regions involved in adaptive neuroplasticity. However, while the relative extent of [^{18}F]FDG uptake in these networks was comparable across both models, synaptic density changes were more pronounced in UVN vs. cUL. Specifically, synaptic density in the vestibular nuclei was significantly lower after UVN, accompanied by a more intense compensatory increase in sensorimotor cortical areas. In conclusion, synaptic density imaging may be a more sensitive method to depict subtle differences in mechanisms of lesion-induced adaptive neuroplasticity than traditional techniques such as imaging of glucose metabolism.

1. Introduction

Dizziness is a symptom that affects 15–30 % of the population at least once in their lifetime (Neuhauser, 2007, 2016). A common cause of acute dizziness is a unilateral vestibulopathy, which can occur due to a preganglionic lesion (e.g., in labyrinthitis) or a postganglionic lesion of vestibular afferents (e.g., in vestibular neuritis) (Zwergal and Dieterich, 2020; Strupp et al., 2022). Irrespective of the lesion localization, patients generally recover over time as adaptive-lesion induced neural plasticity mechanisms become active, thereby compensating for the imbalance. However, it is not well understood if the spatio-temporal trajectories of structural and functional neuroplasticity differ as a result of the lesion intensity and localization. Preclinical models of acute unilateral vestibulopathy are well-suited to study this question: in

* Corresponding author at: Marchioninistraße 15, 81377 Munchen, Germany.
E-mail address: Andreas.Zwergal@med.uni-muenchen.de (A. Zwergal).

https://doi.org/10.1016/j.neuroimage.2026.121821
Received 12 September 2025; Received in revised form 11 February 2026; Accepted 18 February 2026
Available online 19 February 2026

unilateral vestibular neurectomy (UVN), the vestibulocochlear nerve is transected between Scarpa's ganglion and the brainstem entry zone, thus representing a model for complete postganglionic deafferentation (Péricat et al., 2017; Marouane et al., 2020). In contrast, chemical unilateral labyrinthectomy (cUL) uses ototoxic substances, which are injected transtympanically into the middle ear and damage the vestibular and cochlear hair cells by diffusion to the inner ear (Kaufman et al., 1993; Vignaux et al., 2012; Zwergal et al., 2016; Antons et al., 2022, 2023). This preganglionic lesion is considered as an incomplete deafferentation model, because the structural integrity of the vestibular nerve afferents remain intact including some degree of resting discharge (Vignaux et al., 2012). Both models induce acute vestibular symptoms after surgery, such as barrel rolling, head tilt, postural asymmetry, or nystagmus, which suggests a similar functional consequence for central vestibular asymmetry (Beck et al., 2014; Péricat et al., 2017; Rastoldo et al., 2022; Antons et al., 2023). Previous histological studies mostly at the level of the vestibular nuclei have demonstrated a divergent pattern of central compensation in cUL and UVN. It is proposed that the Wallerian degeneration starting from the transected nerve stump in UVN leads to a higher concentration of pro- and anti-inflammatory molecules required for the proliferation, migration, differentiation, and survival of new cells compared to cUL with intact vestibular nerve afferents (Dutheil et al., 2011; Tighilet and Chabbert, 2019; Simon et al., 2020). Furthermore, it is hypothesized that UVN may induce more severe synaptic, i.e., structural reorganization than cUL.

The aim of the present study was to compare the preganglionic cUL and postganglionic UVN rat model using a longitudinal dual-tracer approach with ^{18}Fluorine-fluorodeoxyglucose ([^{18}F]FDG) uptake as a surrogate for functional plasticity and [^{18}F]UCB-H binding for synaptic density. We hypothesized that the synaptic tracer [^{18}F]UCB-H would be more sensitive to depict differences in vivo in the whole-brain lesion-induced structural reorganization compared to [^{18}F]FDG as a marker for functional adaptation. As a more general secondary aim, we wanted to validate whether [^{18}F]UCB-H has the potential to trace structural neuroplasticity in a model of peripheral-nerve damage.

2. Materials and methods

2.1. Ethics

All the experiments were approved by the Government of Upper Bavaria and conducted in accordance with the guidelines for the use of living animals in scientific studies and the German Law for the Protection of Animals (ROB-55.2–2532.Vet_02–20–191).

2.2. Animals and housing

Twenty-four male Sprague Dawley rats (Charles River, Sulzfeld, Germany, mean age 9.5 weeks at the time of the surgery) were divided equally into cUL ($n = 12$) and UVN ($n = 12$). Rats were housed in pairs in individually ventilated cages (IVC) of the double-decker type GR1800 (Tecniplast, Germany) in a humidity and temperature-controlled environment with a 12-hour light/dark cycle. They had free access to water and food, tunnels, cardboard houses, and sticks to gnaw on.

2.3. Experimental procedure

Upon arrival, the animals were given one week to acclimate to their new environment and the experimenter. Over the course of nine weeks, [^{18}F]FDG and [^{18}F]UCB-H positron emission tomography/ computer tomography (PET/CT) scans were performed, accompanied by behavioral tests (Fig. 1). Baseline scans with [^{18}F]UCB-H and [^{18}F]FDG were performed after the adaptation period. The animals were allowed to individually explore the open field set-up once before their behavioral baseline tests in order to accustom them to the setup. [^{18}F]FDG was measured post-operatively on day 1, then weekly until the fourth week. The tracer [^{18}F]UCB-H was chosen as a marker for synaptic density, as the tracer binding to SV2A reflects synaptic density (Serrano et al., 2019, 2020). The synaptic density was evaluated at four time points, once before the surgery (baseline) and postoperatively at week 1, week 3 and week 9. A previous study with the same dual tracer approach in the bilateral chemical labyrinthectomy model revealed that synaptic density is affected predominantly during the end of the experiment at week 9, while the regional cerebral glucose metabolism is altered starting from day 1 with the greatest changes in the first postoperative week (Antons et al., 2022). In addition, open field and clinical scoring on the first three days after surgery and once a week until week 9 assessed the rats' behavior. Postoperative treatment with meloxicam and marbofloxacin was administered after behavioral assessment and PET acquisition to avoid a potential influence on behavior or tracer binding.

2.4. Chemical unilateral labyrinthectomy

Surgery was performed according to previous studies (Beck et al., 2014; Günther et al., 2015; Zwergal et al., 2016, 2017; Lindner et al., 2019; Antons et al., 2022; Zwergal et al., 2022, 2023). For analgesia, animals received metamizole (100–250 mg/kg, s.c.) and the local anesthetic bupivacaine (500 µl of 0.5 % bupivacaine solution, s.c.) and marbofloxacin (2 mg/kg, s.c.) as an antibiotic. With a retroauricular incision, the external ear canal was exposed and the vestibular lesion was evoked by injecting 20 % bupivacaine solution (150 µl) and 10 % sodium-arsanilate acid (150 µl) transtympanically into the middle ear with subsequent aspiration. The solutions diffused through the oval and round window to the vestibular epithelia in the inner ear and caused dysfunction (Vignaux et al., 2012). The animals were given marbofloxacin (2 mg/kg) and meloxicam (1 mg/kg, s.c.) once a day for the next 3 days postoperatively.

2.5. Unilateral vestibular neurectomy

Neurectomy was performed as described in (Péricat et al., 2017) and a similar analgesic and antibiotic treatment was used as described for

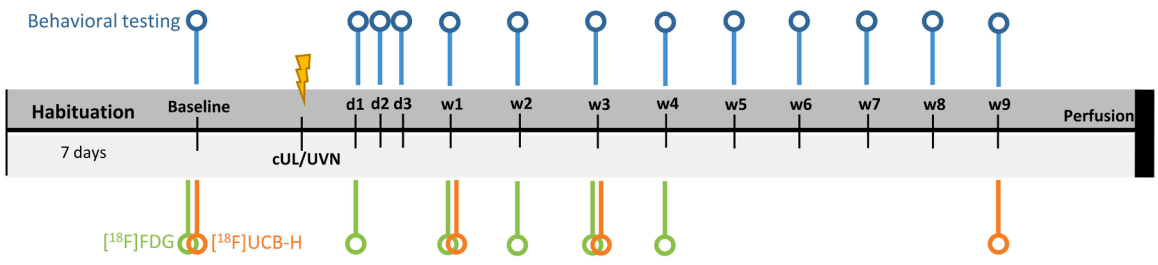

Fig. 1. Overview of the experimental procedure. After a habituation period of seven days, the baseline measurements with [^{18}F]FDG and [^{18}F]UCB-H and behavioral testing started. After cUL/UVN surgery (indicated by the yellow lightning), PET was continued at weeks 1, 3, and 9 for [^{18}F]UCB-H and on day 1, week 1, 2, 3 and 4 for [^{18}F]FDG. Behavior was assessed daily during the first three postoperative days, then weekly until week 9. At the end of the experiment at week 9 the animals were perfused. d = day, w = week.

the cUL. Instead of bupivacaine, lidocaine (4 mg/kg, s.c.) was used as a local anesthetic. After opening the middle ear through the Bulla tympanica and the promontory by drilling, access to the vestibular nerve was created by levering out the cochlea. Subsequently, the vestibulocochlear nerve was transected at its emergence from the brainstem. Postoperative treatment with marbofloxacin and meloxicam was performed as described after cUL.

2.6. Criteria for exclusion

The following criteria led to immediate termination of the experiment. According to these criteria, one animal from the UVN group was excluded because of an absence of symptoms postoperatively.

1. Body weight: loss of >15 % of body weight
2. General condition: trembling, unable to move in a coordinated manner, hunched posture, shallow and labored breathing, cramps, paralysis (trunk muscles, extremities), labored breathing sounds, animal feels cold
3. Behavior: self-isolation, apathy, marked hyperkinetic or behavioral stereotypies, automutilation
4. Model-related symptoms: purulent wound secretions, corneal opacity, corneal ulceration
5. Reactions to therapeutic agents: severe diarrhea
6. Absence of signs of lesion-related symptoms: If there was any doubt about the success of the operation 3 days after surgery due to the absence or severity of symptoms, the animal was removed from the experiment.

2.7. Open field testing

Locomotion behavior was assessed at baseline and on days 1, 2, 3 post-operatively, then weekly up to week 9. Exploratory behavior was recorded in an open field arena (70 × 70 × 36 cm) using the automated software EthoVision XT® 16 (Noldus®, Netherlands). The system tracked the nose point, body center, and tail base using a camera mounted above the arena for a duration of 10 min per session. At the start of each trial, rats were placed in the same location within the arena and allowed to move freely. The arena was illuminated from above with a light intensity of 45–50 lx. Black curtains surrounded the setup to minimize external visual distractions. Parameters recorded included mean velocity, movement, turn angle, and counterclockwise rotations.

2.8. Clinical scoring

In order to evaluate the elicited vestibular syndrome qualitatively, clinical scoring was performed in the first three postoperative days and then weekly. The protocol used in previous studies for clinical scoring (Bergquist et al., 2008) was adapted and the more objective clinical scoring described by Péricat was added instead of the postural asymmetry (Bergquist et al., 2008; Péricat et al., 2017; Zwergal et al., 2017; Lindner et al., 2019; Antons et al., 2022, 2023). Animals were placed in an empty cage and their behavior was videotaped for two minutes and simultaneously recorded on a sheet of paper. Observed parameters of nystagmus, head tilt, and elevation tail rotation test results were weighted with 10 points for the severest symptom manifestation and 1 point for the mildest. In addition, the clinical scoring by Péricat was weighted as following: Barrel rolling was rated with 5 points, retropulsion (backwards movement) with 4 points, circling (circular motions) with 3 points, head bobbing (rocking up and down with the head) with 2 points, and the presence of a head tilt with 1 point. In total, the rat could receive 15 points per session if each behavior was displayed (Péricat et al., 2017). Two experimenters did the behavioral examination, one was blinded and rated the behavioral parameters of clinical scoring, head tilt, and elevation tail rotation test based on randomized videos. Finally, the calculated mean between the experimenters was used for further statistical analysis.

2.9. PET/CT imaging

For tracer injection, the animals were anesthetized with 2 % isoflurane in O_2 (1–2 l/min) and a 24-gauge catheter was placed in the lateral tail vein. Then 40 MBq of tracer diluted in 0.5 ml NaCl was injected, the animals were allowed to wake up and move freely. After an uptake time of 20 min, they were re-anesthetized with isoflurane and placed in the μPET/CT (nanoScan® PET/CT, MedisoMedical Imaging Systems®, Hungary). Here they received a continuous isoflurane-oxygen mixture, heated air, and their vital parameters were monitored. After CT acquisition for attenuation correction, the PET was started exactly 30 min post injection. The following PET acquisition took 30 min; both [^{18}F]FDG and [^{18}F]UCB-H scans were performed as static scans. In weeks when both [^{18}F]FDG and [^{18}F]UCB-H were measured, at least one day was allowed to elapse between the two scans to eliminate any residual tracer activity and to allow the animal to recover from anesthesia.

2.10. Image processing and statistical analysis

PET images were reconstructed using Nucline nanoScan software and corrected for radioactive decay, scatter, attenuation, dead time, and sensitivity normalization. The resulting images had a voxel size of 0.4 × 0.4 × 0.4 mm^3 and consisted of 212 × 212 × 235 voxels. Image preprocessing was performed using PMOD image analysis software (v4.004, PMOD Technologies, Zurich, Switzerland). The brain was centered by cropping the images, followed by application of an isotropic Gaussian filter (0.4 mm FWHM). Images were then co-registered to the Schiffer Px rat atlas (Schiffer et al., 2006). The images were normalized by calculating the standardized uptake value ratio by global mean normalization (SUV_R), the brain was segmented into 36 brain regions based on the Schiffer Px rat atlas, and mean normalized activity values were extracted for each region. Global mean normalization (SUV_R) was chosen because it performed better than SUV normalization. With SUV normalization, the animal's body weight and the injected dose were taken into account. By comparing these two normalization methods for a reference region (left insular cortex, < 5 % change compared to baseline in both [^{18}F]FDG and [^{18}F]UCB-H PET) SUV_R normalization performed better with a lower coefficient of variance than SUV-normalization or pre-normalization (Supplementary Figure 1).

2.11. Statistics

Mean normalized activity values (SUV_R) were extracted for each segmented brain region at baseline (BL), day 1 (d1) and weeks (w) 1, 2, 3, 4 and 9 post-surgeries. [^{18}F]UCB-H served as a surrogate for synaptic density.

Behavioral and PET-data were analyzed and visualized using GraphPad Prism (v10.1.2 for windows GraphPad Software, San Diego, CA, USA). Eighteen bilateral brain regions were selected based on their involvement in vestibular and motor processing, as demonstrated in previous work by this group (e. g. Lindner et al., 2019; Antons et al., 2022, 2023). First, a difference in baseline SUV_R values between UVN and cUL was calculated for each brain region and each tracer using a two-way ANOVA with Šidák correction for post-hoc comparisons. A p-value of 0.05 was considered significant. Since there were no statistical differences between the groups at baseline, it was reasonable to pool the baseline values for [^{18}F]FDG and [^{18}F]UCB-H (see Supplementary Figures 2 and 3). This approach increased the statistical power and precision of subsequent comparisons by enlarging the reference dataset. Subsequently, behavioral data and PET data were analyzed using a maximum likelihood (REML) mixed-effects model. Post-hoc comparisons were conducted using Šidák correction for multiple testing. Statistical significance was defined as $p < 0.05$.

For the behavioral data, the fixed effects included "Time" and

"Surgery method", as well as their interaction ("Time x Surgery method"). The random effect was the individual animal.

For the PET data, the fixed effects were "Time" and "Brain regions" and their interaction ("Time x Brain regions"). The random effect was the individual animal. Postoperative time points were compared to the pooled baseline values across each group (BL vs. d1, d2, d3, w1, w2, w3, w4 and w9). Additionally, comparisons between the two groups at each time point per brain region were performed (UVN vs. cUL).

The relative change of activity (ΔSUV_R) at each postoperative time point compared to pooled baseline was calculated using the following formula

$$\Delta SUV_R = \frac{SUV_{R\,timepoint\ post} - SUV_{R\,Baseline}}{SUV_{R\,Baseline}}\ x\ 100\ \%$$

Changes were classified as follows:

- Mild: 5–10 %
- Moderate: 10–15 %
- Severe: > 15 %

Significance levels were indicated using asterisks (* $p < 0.05$, ** $p < 0.01$, *** $p < 0.001$).

Two-tailed Pearson's correlation coefficient was applied to week 9 [^{18}F]UCB-H SUV_R for the left and right vestibular nucleus (VN) and the bilateral motor cortex in cUL and UVN respectively. Only these four regions were chosen, because they are considered to be mainly influenced by acute unilateral vestibulopathy, with the left more than right VN as a landmark for infratentorial changes and the motor cortex for supratentorial. In addition, [^{18}F]UCB-H SUV_R in these regions was also correlated with clinical scoring results at different time points. A p-value of 0.05 was considered significant.

In addition, exploratory voxel-wise analyses were conducted using SPM12 implemented in Matlab. A two-way *t*-test was performed with a significance threshold of $p < 0.005$ (uncorrected), without threshold masking or multiple comparison correction, and an extended threshold of 20 contiguous voxels. The graphs generated with SPM show the voxel-wise t-test statistics obtained from the statistical parametric mapping analysis.

3. Results

3.1. Statistical voxel-wise whole-brain analysis in all animals

Both UVN and cUL animals showed a marked reduction of [^{18}F]FDG uptake in the ipsilesional VN compared to baseline (Fig. 2A). In the UVN group, this decrease was visually more pronounced on day 1 and extended to the contralesional VN over the course of four weeks compared to the cUL group. However, when directly comparing UVN with cUL (Fig. 2B), no significant differences could be detected.

In contrast to these subtle changes in [^{18}F]FDG uptake, synaptic loss in the vestibular nuclei was more pronounced in the UVN group, when compared to baseline (Fig. 3A). After neurectomy, the animals had a significant decline in synaptic density at week 1, which further decreased until week 9. Additionally, the synaptic loss extended to the cerebellum. In contrast, the cUL showed more subtle changes that were only visible at week 9. These differences were also apparent when directly comparing UVN with cUL (Fig. 3B): UVN had less uptake of [^{18}F]UCB-H in the vestibular nuclei (peak at week 1) and cerebellum (peak at week 9).

In [^{18}F]FDG PET, the thalamus, basal ganglia, somatosensory cortex, and motor cortex were more upregulated in the UVN animals than in the cUL mostly on day 1 (Fig. 4A). These disparities rapidly declined, except for the thalamus and somatosensory cortex, where an increased glucose metabolism in the UVN was still present at week 2.

Direct group comparisons revealed higher [^{18}F]UCB-H uptake in the UVN group in several regions at week 1, including the thalamus, basal ganglia, somatosensory cortex, and motor cortex (Fig. 4B). While synaptic density in the thalamus decreased continuously following an initial peak at week 1, it remained stable in the basal ganglia. Synaptic density in the somatosensory cortex reached a peak at week 3, and at week 9 in the motor cortex.

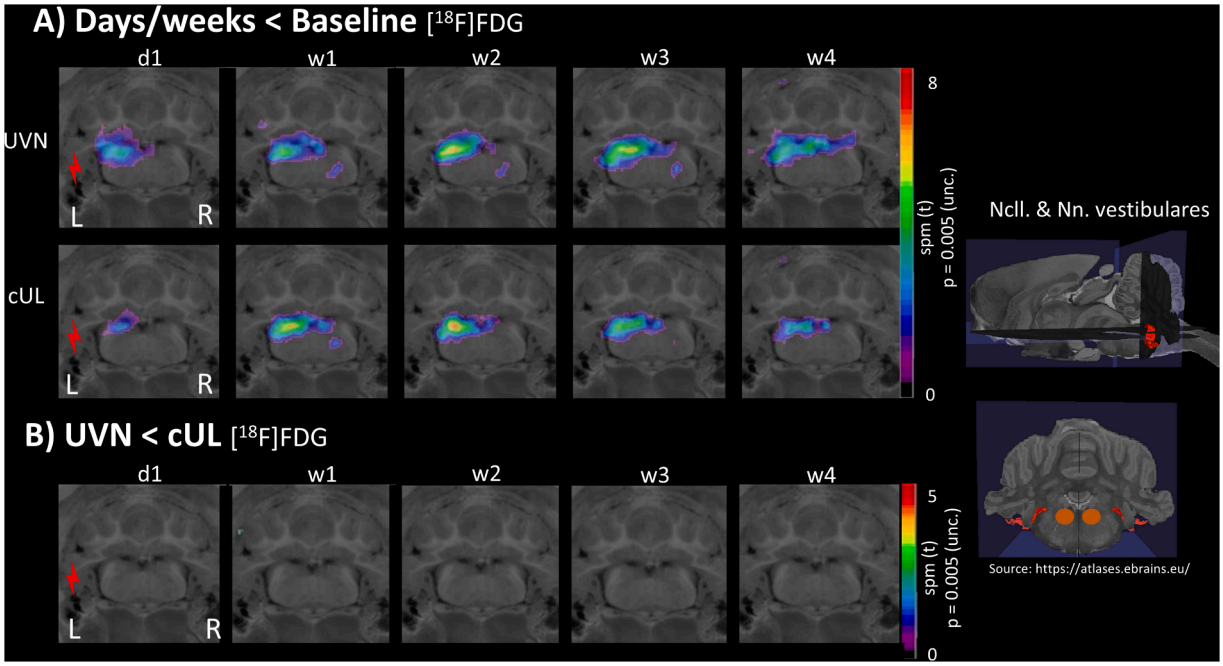

Fig. 2. Decrease of [^{18}F] FDG uptake in the vestibular nuclei. A) Each day/week of UVN (n = 11) and cUL ($n = 12$) was compared to baseline and **B)** UVN was compared to cUL. T-values were obtained from voxel-wise *t*-tests comparing each time point to baseline and cUL. A significance threshold of $p < 0.005$ (unc.) was selected and the significant changes were shown with an extended threshold of $k = 20$ voxels. Ncll. = Nuclei, Nn. = Nervi, red flash = intervention site.

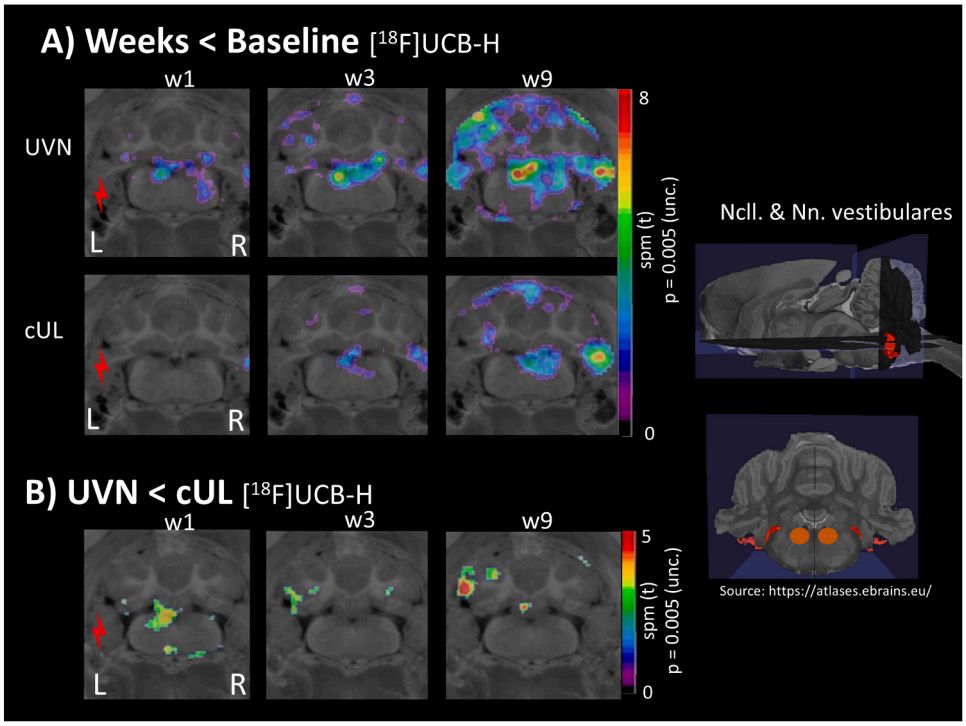

Fig. 3. Decrease of synaptic density in the vestibular nuclei and cerebellum. A) Each week of UVN ($n = 11$) and cUL ($n = 12$) was compared to baseline and **B)** UVN was compared to cUL. T-values were obtained from voxel-wise *t*-tests comparing each time point to baseline and cUL. A significance threshold of $p < 0.005$ (unc.) was selected and the significant changes were shown with an extended threshold of k = 20 voxels. Ncll. = Nuclei, Nn. = Nervi, red flash = intervention site.

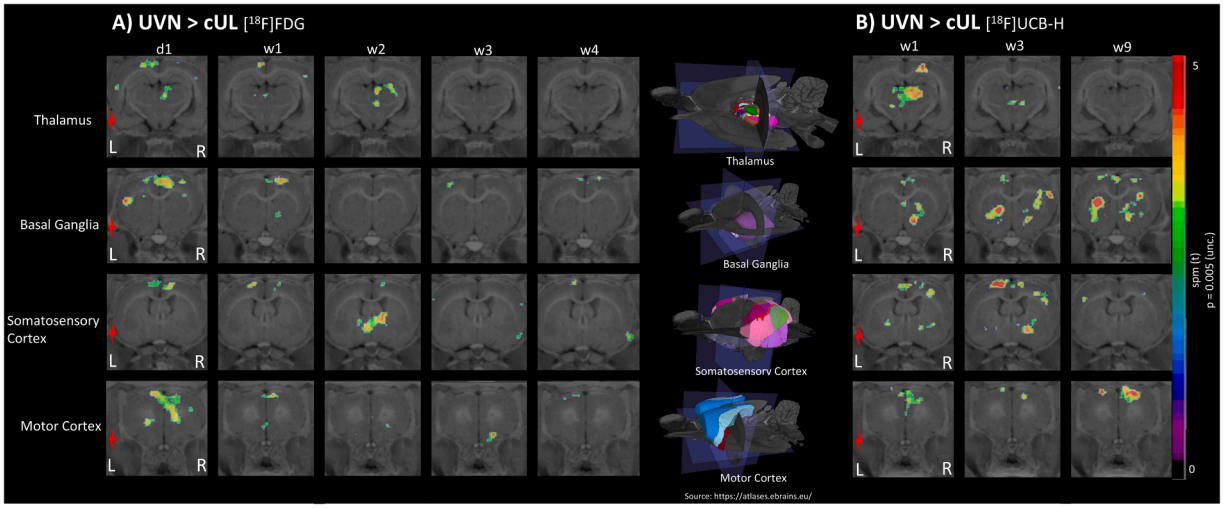

Fig. 4. Increase of A) [^{18}F] FDG uptake and B) synaptic density in the thalamus, basal ganglia, somatosensory cortex, and motor cortex. T-values were obtained from voxel-wise *t*-tests comparing UVN ($n = 11$) with cUL ($n = 12$). A significance threshold of $p < 0.005$ (unc.) was selected and the significant changes were shown with an extended threshold of $k = 20$ voxels, red flash = intervention site.

3.2. [^{18}F]FDG and [^{18}F]UCB-H activity in 36 vestibular and sensorimotor brain regions

Eighteen bilateral brain regions were statistically compared with the baseline using a mixed-model with post-hoc Šidák correction for multiple testing. In the cUL group, all fixed effects had a significant impact on the [^{18}F]FDG uptake (cUL: Time: $F = 7.501$, $p < 0.001$, $\varepsilon = 0.758$; Brain region: $F = 137.1$, $p < 0.001$; Time x Brain region: $F = 4.547$, $p < 0.001$). The same applied to the UVN group (Time: $F = 2.850$, $p = 0.036$, $\varepsilon = 0.599$; Brain region: $F = 196$, $p < 0.001$; Time x Brain region: $F = 3.682$, $p < 0.001$).

For the assessment of synaptic density, all fixed effects had a significant impact in both the cUL (Time: $F = 11.69$, $p < 0.001$, $\varepsilon = 0.913$; Brain region: $F = 153.8$, $p < 0.001$; Time x Brain region: $F = 4.005$, $p < 0.001$) and the UVN group (Time: $F = 13.97$, $p < 0.001$, $\varepsilon = 0.922$; Brain Region: $F = 162.6$, $p < 0.001$; Time x Brain region: $F = 6.862$, $p < 0.001$).

A summary of the relative changes in [^{18}F]FDG uptake for both groups is provided in Supplementary Figure 4 and for [^{18}F]UCB-H uptake in Supplementary Figure 5. All values are reported as mean $SUV_R \pm$ standard deviation or as relative change of SUV_R (% compared to baseline $\pm$ standard deviation).

3.2.1. Brainstem nuclei

The vestibular nuclei displayed a similar [^{18}F]FDG uptake in both groups. Specifically, the left VN showed a significant reduction in [^{18}F]FDG uptake on day 1 compared to baseline (Supplementary Figure 4; UVN: −13.655 % ± 6.876, p = 0.011; cUL: -3.677 % ± 5.058, p = 0.318). When directly comparing the SUV_R of the groups (Fig. 5A and B), the UVN animals demonstrated significantly lower [^{18}F]FDG uptake in the left VN on day 1 (UVN: 1.242 ± 0.085; cUL: 1.385 ± 0.07; p = 0.039).

This metabolic reduction was accompanied by a loss of synaptic density (Fig. 5C and D). Compared to baseline, only the UVN group displayed a highly significant decrease of >5 % in the left VN at week 1 (Supplementary Figure 5; -5.793 % ± 4.078, p = 0.002), which persisted until week 9 (-7.469 % ± 4.187, p = 0.001). In contrast, the cUL group showed a reduction of >5 % only in the right VN at week 9 (−8.587 % ± 6.483, p < 0.001). In a direct comparison (Fig. 5C and D), only the left VN is significantly less activated in the UVN group at week 1.

The right inferior colliculus also showed a strongly reduced [^{18}F]FDG uptake of 10–15 % from week 1 to week 4 in both surgery groups, however, in the UVN the left inferior colliculus was upregulated at week 1, 2, and 4 in comparison to baseline (Supplementary Figure 4).

3.2.2. Cortical areas and basal ganglia

In the UVN group, a significant increase in [^{18}F]FDG uptake of >5 % compared to baseline was observed in the left visual cortex on day 1 (5.078 % ± 3.437, p = 0.023). A direct comparison of the SUV_R between groups revealed significantly higher [^{18}F]FDG uptake in the right motor cortex in UVN animals on day 1 (UVN: 1.097 ± 0.049; cUL: 1.038 ± 0.042; p = 0.033; see Supplementary Figure 6).

Synaptic density increased similarly in cortical regions across both groups when compared to baseline. However, the UVN showed an additional, sustained increase in the prefrontal cortex from week 3 to week 9. Notably, at week 9, the relative increase in synaptic density in the frontal association cortex was nearly twice as high in the UVN group compared to the cUL group (UVN: left 13.942 % ± 6.939, right 12.432 % ± 10.102; cUL: left 6.947 % ± 8.071, right: 8.105 % ± 8.984; see Supplementary Figure 5). Furthermore, the basal ganglia appeared to be more prominently involved in structural neuroplasticity in the UVN group, showing upregulation of synaptic density in the striatum at week 9 (Fig. 5G and H). At week 9, the Pearson's correlation coefficient revealed a strong negative correlation for SUV_R of the left VN and the left motor cortex for the UVN (see Supplementary Figure 7): A loss in synaptic density in the left VN (indicated by low SUV_R values) is accompanied by an upregulation of SV2A binding in the motor cortex (left motor cortex: r = −0.787, p = 0.004; right motor cortex: r = −0.351, p = 0.29). The cUL animals did not show this interrelation (left motor cortex: r = 0.164, p = 0.611; right motor cortex: r = 0.018, p = 0.955). This ipsilesional divergent pattern on infratentorial loss and supratentorial gain of synapses was only visible for the left vestibular nuclei, as the right vestibular nuclei did not show any relevant correlations (Supplementary Figure 7C and D).

3.3. Behavioral testing

UVN and cUL exhibited the typical symptoms of unilateral vestibular dysfunction, including barrel rolling, retropulsion, circling, head bobbing, and head tilt. No statistically significant differences between the two groups were found for most parameters, with the exception of nystagmus and head tilt (Fig. 6). On day 1, cUL rats showed a significantly milder head tilt compared to the UVN rats (Time: F = 59.04, p < 0.001, ε = 0.345; Time x Surgery method: F = 4.698, p < 0.001; multiple comparisons between UVN and cUL at d1: p < 0.001; Fig. 6B).

Additionally, symptom progression assessed using the Péricat clinical scoring system revealed a transient secondary peak on day 2 in the cUL animals (Time: F = 70.34, p < 0.001, ε = 0.368; Fig. 6A). Compared to the cUL group, UVN rats showed markedly reduced or absent nystagmus during the first two postoperative days (Time: F = 41.41, p < 0.001; Surgery method: F = 36.41, p < 0.001; Time x surgery method: F = 15.76, p < 0.001; multiple comparisons between UVN and cUL at AW: p < 0.001; day 1: p < 0.001; day 2: p < 0.001; Fig. 6D). The elevation tail rotation test did not reveal any significant disparities between the two surgery groups, although the UVN reached the maximum of 10 points directly after awakening and the cUL only after one week. Consequently, the decline of the turning events assessed by the elevation tail rotation test commenced earlier in the UVN.

The correlation of the clinical scoring with the SUV_R values of the synaptic density at week 9 in the motor cortex and vestibular nuclei revealed positive correlations. For the left motor cortex, the only significant correlation could be found in the UVN group at week 4 (r = 0.696, p = 0.017, Supplementary Figure 8A). In the right motor cortex, the synaptic density positively and significantly correlated in the UVN group at week 8 (r = 0.830, p = 0.002, Supplementary Figure 8B) and week 9 (r = 0.622, p = 0.041, Supplementary Figure 8C). In the vestibular nuclei the correlations did not reveal any significant results for both surgery groups.

Open field testing did not reveal a significant difference in exploratory behavior between the two surgery methods (Fig. 7). Both surgical models induced a significant reduction in locomotion speed (mean velocity) on days 1 and 2 relative to baseline (Time: F = 14.54, p < 0.001, ε = 0.290; UVN d1: p < 0.001; cUL d1: p < 0.001, d2: p = 0.001; Fig. 7A). This reduction in activity was mirrored by a significant increase in the percentage of time spent immobile (Time: F = 14.03, p < 0.001, ε = 0.3461; UVN: d1: p < 0.001, d2: p = 0.048; cUL: d1: p < 0.001, d2: p < 0.001; Fig. 7B). Furthermore, a significant increase in counterclockwise rotations, i.e., towards the lesioned side, was observed after the surgery (Time: F = 3.750, p = 0.031, ε = 0.169; Fig. 7C). This was paralleled by an increase of the relative turn angle, with positive values indicating a tendency towards the lesioned left side (Fig. 7D).

4. Discussion

The key findings of this dual-tracer longitudinal imaging study in a pre- and postganglionic unilateral vestibular lesion model were the following: 1) Behavioral recovery from acute vestibular asymmetry as an indication of functional central compensation was roughly similar in both models. 2) Accordingly, [^{18}F]FDG uptake changes after UVN and cUL showed no differences for the later imaging time points after surgery (i.e., weeks 2–4). 3) In contrast, SV2A imaging displayed a more severe synaptic density loss in the vestibular-cerebellar brainstem hubs in UVN, which were accompanied by more pronounced increases of synaptic density in cortical sensorimotor areas. In conclusion, SV2A imaging was more sensitive to depict alterations of adaptive neuroplasticity than [^{18}F]FDG in a peripheral-nerve lesion model.

Despite the different lesion mechanisms in UVN and cUL, the spatial distribution of both functional and structural adaptive neuroplasticity was similar with involvement of brain areas previously recognized as being involved in vestibular compensation (e.g., the cerebellum), sensory substitution (e.g., the thalamus), and motor adaptation (e.g., the motor cortex and striatum). These findings speak for relatively conserved network-based mechanisms of central vestibular plasticity. Accordingly, dynamics of behavioral recovery were similar in UVN and cUL. The behavioral characteristics in our study are in accordance with the existing literature (Péricat et al., 2017; Zwergal et al., 2017; Lindner et al., 2019; Rastoldo et al., 2020, 2022; Antons et al., 2023). Direct comparison of cUL and UVN in a mouse model suggested more acute symptoms in UVN, similar to our findings, while behavioral recovery was irrespective of the lesion mechanisms (Simon et al., 2020). Thereby, both deafferentation models seem to be robust to investigate mechanisms of central vestibular compensation.

However, the lesion mechanism with its inherent difference in the extent of deafferentation (e.g., complete in UVN vs. incomplete in cUL), resulted in differences in the time trajectories of neural plasticity

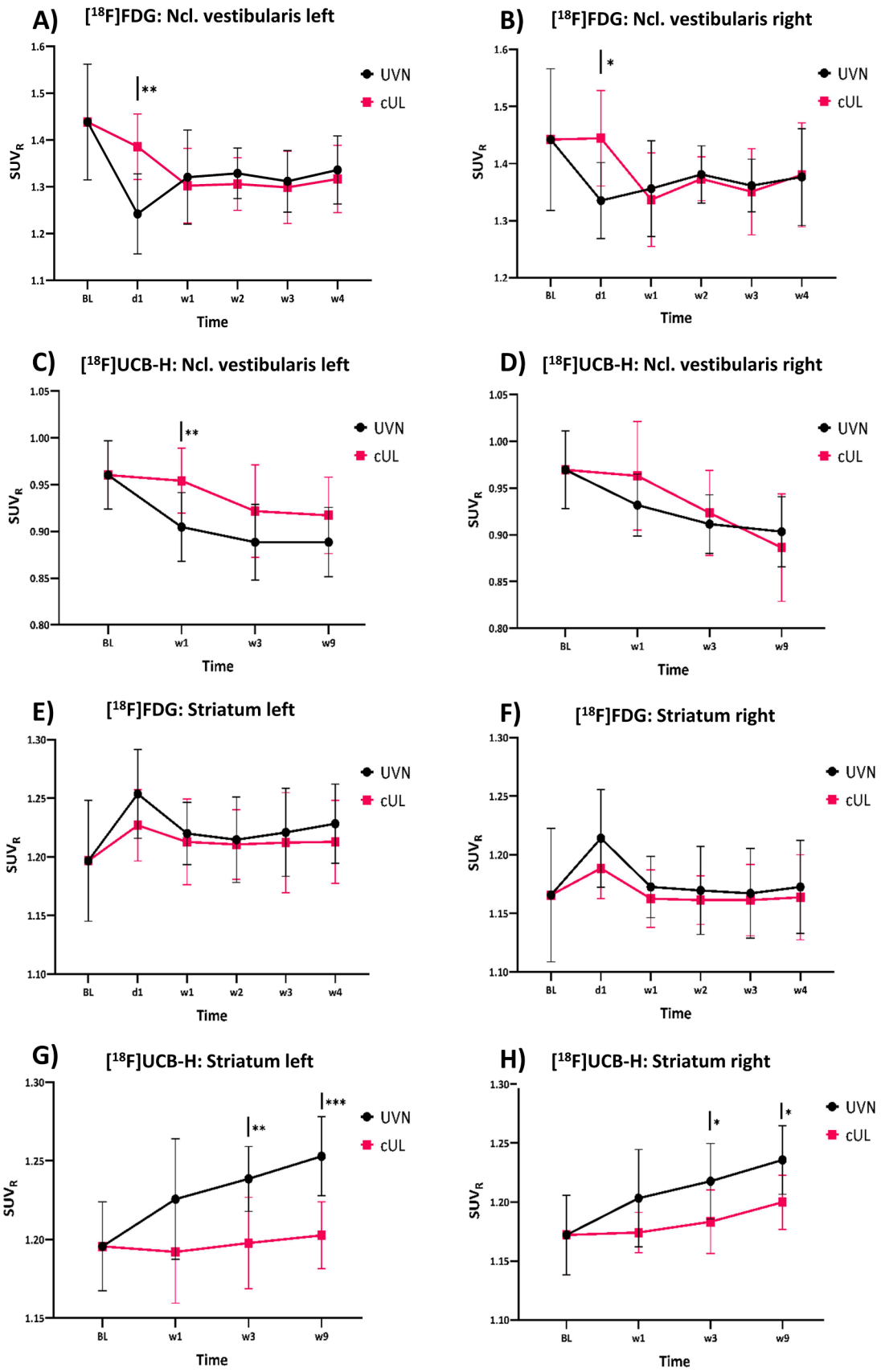

Fig. 5. Change of [^{18}F] FDG uptake and synaptic density ([^{18}F] UCB-H) in vestibular and motor brain regions. A-D) [^{18}F]FDG uptake and synaptic density in the vestibular nuclei, **E-H)** [^{18}F]FDG uptake and synaptic density in the striatum. The values are presented as mean of mean normalized activity values (SUV_R) with standard deviation. BL = baseline, *w* = week, Ncl. = nucleus * $p < 0.05$, ** $p < 0.01$, *** $p < 0.001$.

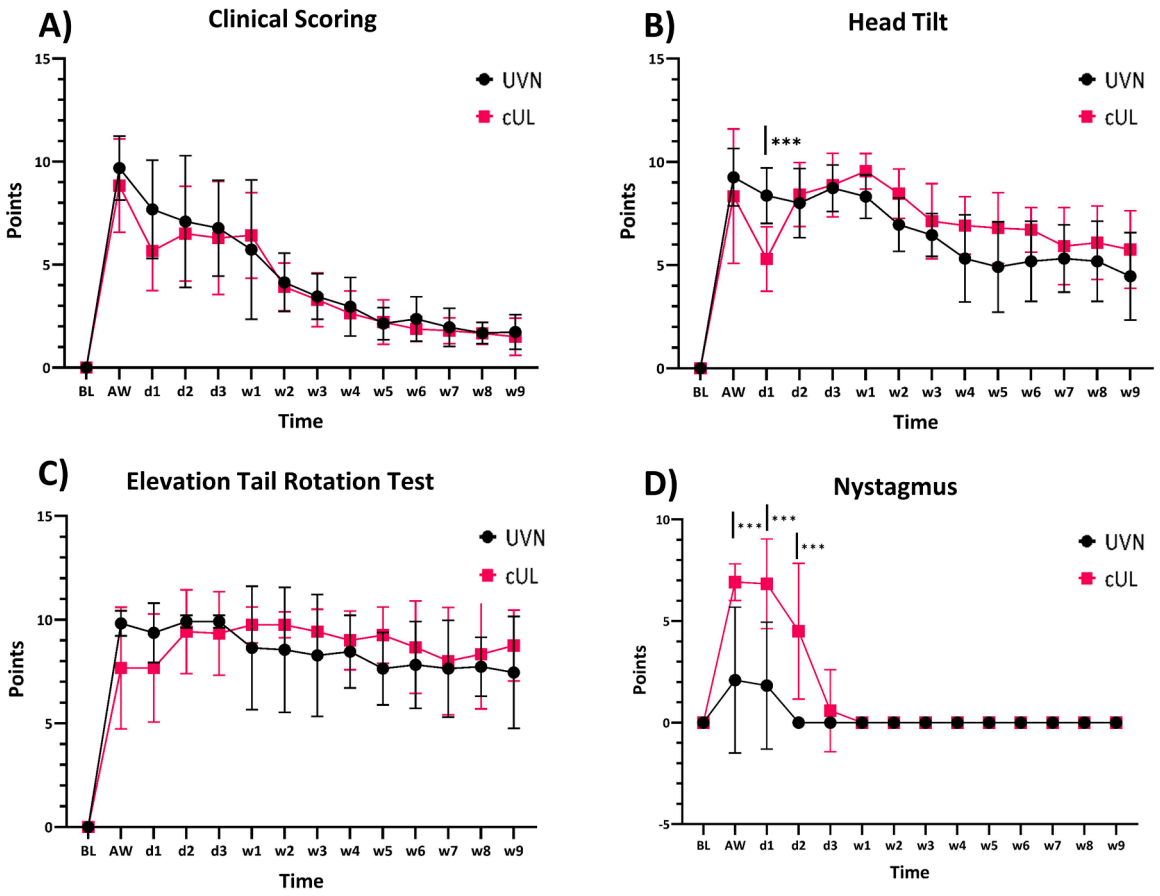

Fig. 6. Behavioral tests including **A)** Clinical Scoring according to the Péricat et al. (2017) protocol, **B)** head tilt, **C)** elevation tail rotation test, and **D)** nystagmus of UVN ($n = 11$) and cUL ($n = 12$) over 9 weeks. Data are presented as means with standard deviation. BL = baseline, AW = awakening, d = day, w = week. * $p < 0.05$, ** $p < 0.01$, *** $p < 0.001$.

mechanisms between the models. Importantly, these differences were only minor and transient for changes in [^{18}F]FDG uptake, but more pronounced and enduring for changes in synaptic density.

This can most clearly be exemplified in the first ipsilesional central vestibular hub, i.e., the left VN: While [^{18}F]FDG uptake decreased both for cUL and UVN over time compared to the baseline respectively, there were transient differences of the [^{18}F]FDG uptake for both models on day 1 only. This finding may reflect the instantaneous deafferentation mechanism of UVN compared to a more delayed onset effect of the ototoxic cUL model. On the other hand, later on, functional compensation mechanisms in the vestibular nuclei may be similar across both models, which speaks for a sufficient static compensation mechanism at a brainstem level irrespective of the deafferentation mechanism.

In contrast, the UVN rats exhibited a more significant synaptic loss in the ipsilesional VN by week 1 in comparison to the cUL, which further increased and extended to the cerebellum until week 9. This finding is in accordance with the neurobiological assumption that UVN results in a secondary Wallerian degeneration followed by synaptic loss of nerve terminals, compared to a less significant degradation of synapses in cUL, which is driven not by structural damage but rather by a loss of functional vestibular input. The significant drop in [^{18}F]UCB-H uptake after UVN is in accordance with previous immunohistochemical studies in different animal models: in a UVN cat model, a loss of 35 % of synapses in the ipsilesional VN occurred 3 weeks after the lesion, which subsequently improved to a 14 % loss relative to baseline after 9 weeks, speaking for some degree of synaptic reoccupation (Raymond et al., 1991). In a *Xenopus laevis* lesion model with removal of the vestibular nerve including the Scarpa's ganglion, the number of nerve terminals in the ipsilesional vestibulocochlear nucleus was significantly reduced seven days after surgery (Lambert et al., 2013). Similarly, a unilateral cochlear ablation resulted in a synaptic reduction to 54 % in the ipsilesional cochlear nucleus (Hildebrandt et al., 2011). In comparison, the extent of decrease of SV2A binding in our study was lower, equaling about 5–10 %, and more persistent without evidence for a synaptic reoccupation within 9 weeks post UVN. Naturally, SV2A imaging may not reach the granularity of immunohistochemical analysis of synaptic density, but has the advantage of representing a valid marker for longitudinal *in vivo* analysis of lesion-induced synaptic density changes.

Interestingly, dual-tracer imaging depicted not only relative decreases in [^{18}F]FDG uptake and SV2A binding in brainstem-cerebellar circuits, but also relative increases in supratentorial sensorimotor networks. This may be interpreted as an adaptive neuroplasticity mechanism to substitute and adapt to the peripheral vestibular lesion. Similar findings have been previously made in a bilateral chemical labyrinthectomy model, where an upregulation of [^{18}F]FDG and SV2A binding was, for instance, found in the thalamus (Antons et al., 2022). While the increase in [^{18}F]FDG uptake in higher sensorimotor networks was transient (day 1), synaptic density changes in these areas were more persistent, especially in the UVN group. Previous studies have shown a remodeling of neuronal representation in the somatosensory cortex following UVN in the rat (Facchini et al., 2021) and a change in motor cortex connectivity after cUL (Grosch et al., 2021). Consequently, SV2A seems to be able to depict also secondary adaptive neuroplasticity changes in remote networks during active adaptation with a higher sensitivity than [^{18}F]FDG. The findings of the current study further indicate that SV2A imaging can also robustly depict relative increases in synaptic density, while its previous applications were mostly focused on disorders with an abundant synaptic loss (e.g., dementia, parkinsonian

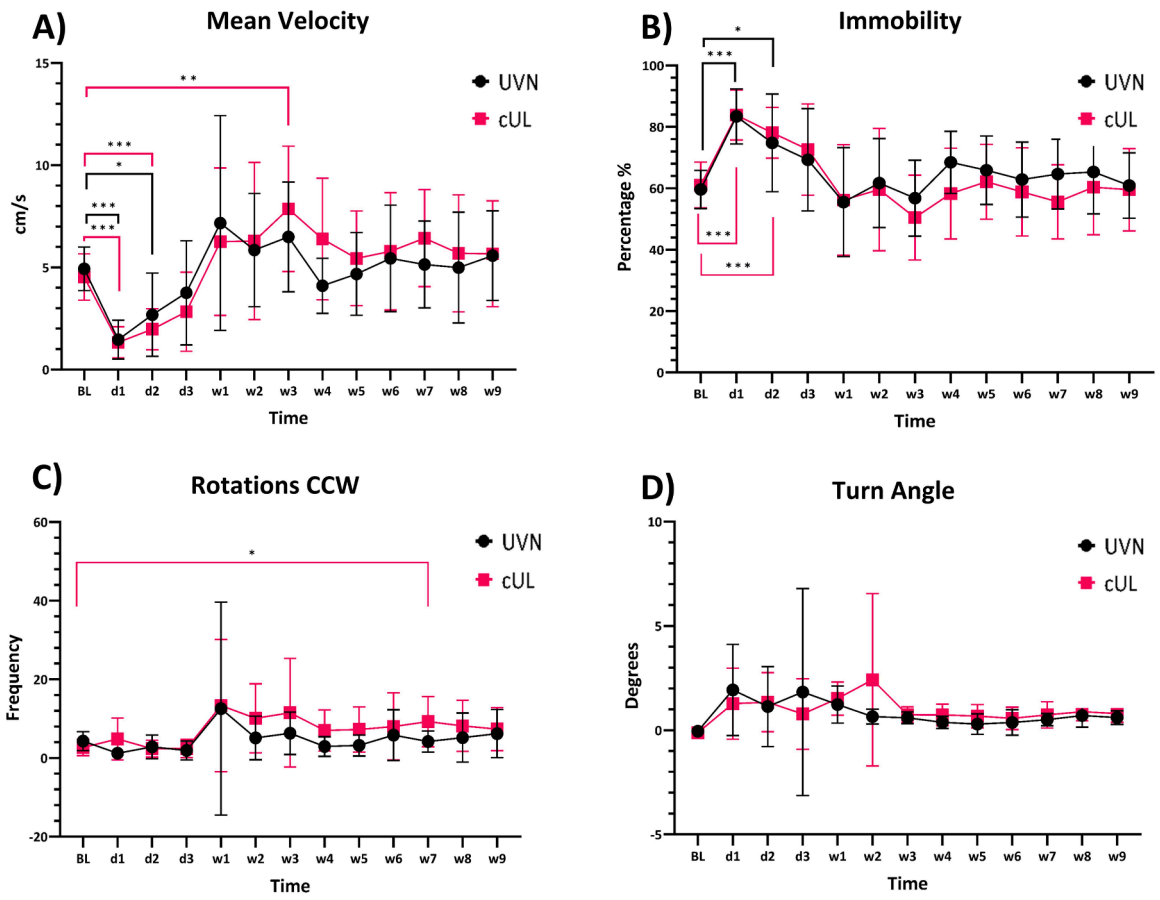

Fig. 7. Behavioral assessment in the open field of the UVN ($n = 11$) and cUL ($n = 12$) groups over 9 weeks. The parameters **A)** mean velocity, **B)** immobility, **C)** rotation counterclockwise (CCW), and **D)** turn angle were analyzed. Data are presented as means with standard deviation. BL = baseline, d = day, w = week. * $p < 0.05$, ** $p < 0.01$, *** $p < 0.001$.

syndromes) (Carson et al., 2022; Howes et al., 2024).

Synaptic loss in the ipsilesional VN and an increase in synaptic density in cortical motor networks seem to occur in conjunction. The strong negative correlation between the left VN and the left motor cortex at week 9 in the UVN group indicates that synaptic loss at the infratentorial level may be an active driver of sensorimotor adaption in the supratentorial hubs during vestibular compensation. It should be noted that this correlation did not appear for the cUL group. This may be specifically due to the type of lesion: The postganglionic lesion achieved by UVN results in an abrupt and complete loss of structural integrity of the first vestibular neuron and functional input to the central vestibular circuitry compared to cUL. As a result, the pressure to replace this missing vestibular input is transferred to connected supratentorial levels, thus increasing the extent of adaptive neuroplasticity. Here, we should mention the side-specificity of the coupling of the VN to supratentorial networks. In rats, Best and colleagues revealed a dominance of the left hemisphere for vestibular processing (Best et al., 2014). In humans, functional imaging studies speak for a predominant ipsilateral ascending projection of vestibular inputs to vestibular insular networks and a predominant contralateral ascending projection to multisensory-motor networks (Dieterich et al., 2003; Conrad et al., 2023). Therefore, the upregulated left motor cortex in this study could represent an adaptive mechanism, which is driven by increased inputs from the intact right VN. Notably, further inverse correlations of [^{18}F]UCB-H SUV_R in the left VN were only found for the left visual and olfactory cortex at week 9 (data not shown), again indicating specific mechanisms of active sensory substitution on a cortical level.

This study employed global mean normalization to account for interindividual variability in tracer uptake. However, it has been argued that this type of normalization may bias regional comparisons, particularly in cases where widespread metabolic changes occur (Borghammer et al., 2009). The data-driven normalization method assumes that a large part of the brain remains stable by identifying "non-differing" voxels between groups, which are considered candidates for a reference region. However, in this study the lesions cause widespread neuroplastic changes which violate this assumption. Moreover, the comparison of models focuses on differences in spatial patterns of metabolism and not on absolute metabolic levels. Global mean normalization facilitates comparison of relative metabolic patterns between models with differing overall activity levels, enabling direct interpretation of regionally specific adaptions. In addition, this study analyzed longitudinal PET scans at different time points and different tracers. Data-driven methods can yield different reference masks or scaling factors per time point or tracer, leading to inconsistent comparisons and introducing additional variability.

The reduced [^{18}F]FDG uptake in the right inferior colliculus likely results from the auditory co-lesion inherent to both lesion models rather than vestibular-specific effects. In the UVN model, the cochlea is surgically removed, whereas in the cUL model, the tympanic membrane is punctured and cochlear hair cells are destroyed through the diffusion of sodium-arsanilate acid and bupivacaine. Because the second neuron of the auditory pathway projects contralaterally, this results in reduced metabolic activity in the contralateral inferior colliculus. Therefore, the prominent reduction of [^{18}F]FDG uptake is resulting from the auditory loss and is not connected to the vestibular loss.

Beyond the context of vestibular injury, the enhanced sensitivity of SV2A PET imaging for detecting subtle or long-term synaptic alterations has also been demonstrated in other neurological disease models. In

experimental spinal cord injury, SV2A PET revealed persistent synaptic loss that was not captured by metabolic imaging, underscoring that structural synaptic integrity may deteriorate independently of regional glucose metabolism (Bertoglio et al., 2022). Similarly, in a longitudinal study of patients with Huntington's disease, SV2A PET identified early synaptic decline that remained undetectable with [^{18}F]FDG or volumetric magnetic resonance imaging (MRI) (Delva et al., 2023). These findings align with our observations in the present study, in which synaptic changes were more pronounced than the corresponding metabolic alterations. Together, these complementary reports strengthen the interpretation that SV2A PET provides more direct and sensitive measure of synaptic remodeling.

The relation of synaptic density to behavioral recovery still seems to be complex. As an example, increased synaptic density in the left motor cortex at week 9 was found in rats with a higher symptom load at week 4. Therefore, a higher synaptic density could be an indicator of adaption to more severe symptoms of vestibular asymmetry in the intermediate phase after the peripheral vestibular lesion. This view is also reinforced by the fact that we see a higher increase of synaptic density in cortical sensorimotor region in the UVN model, which is considered to result in a more complete vestibular deafferentation compared to the cUL model. In summary, increase in synaptic density can be an indicator for a higher demand in adaptive neuroplasticity, but may not automatically result in a faster behavioral recovery.

5. Limitations

This study has several limitations. First, only males were included in the study design, as cycle dependent fluctuations of female rats would add variability to locomotor activity, exploratory behavior and potentially metabolic PET signals. The inclusion of both sexes would improve the translational value and generalizability of the findings and will be taken into account in the design of future studies.

Moreover, vestibular lesions are known to induce a transient stress response. As demonstrated by Tighilet and colleagues, the hypothalamo-pituitary-adrenal axis is activated after UVN with increased bilateral expression of stress-related hormones during the acute phase, which normalizes once vestibular compensation is achieved (Tighilet et al., 2009). Accordingly, stress-related effects could potentially influence SV2A binding at early time points (week 1–3 post surgery) when compared to baseline. However, as shown in Supplementary Figure 5, the most prominent changes in SV2A binding occurred in cortical regions around week 9, when the vestibular syndrome is largely compensated. The early ipsilesional decrease of SV2A binding in the vestibular nuclei (week 1) is consistent with a lesion related rather than stress related origin. Moreover, because both models underwent comparable vestibular symptoms and behavioral alterations (see Fig. 6), any generalized stress response would likely have affected both groups similarly and thus cannot account for the between-model differences observed (Figs. 3B and 4). Furthermore, the hypothalamus as a core region for central stress response was not showing any increase in [^{18}F]FDG uptake in the hypothalamus VOI (Supplementary Figure 4). Therefore, no indication for an imaging correlate of stress related activation of the hypothalamo-pituitary-adrenal axis could be found.

And lastly, each rat served as its own control by comparing post-lesional changes to its individual pre-lesional baseline values. With this within-subject approach and the omission of a control group, age-related changes over nine weeks could be a confounding factor. However, no developmental changes in metabolic networks could be detected in [^{18}F]FDG PET or SV2A PET (Xiong et al., 2023) in adolescent and young-adult rats and mice. In our study, baseline [^{18}F]FDG and [^{18}F]UCB-H PET scans were performed at approximately 8 weeks of age and follow up-scans up to 13 weeks ([^{18}F]FDG) and 18 weeks ([^{18}F]UCB-H), which fall within this developmentally stable period.

6. Conclusions

In conclusion, the distinct spatio-temporal dynamics and transregional correlation patterns of SV2A binding represent biologically plausible mechanisms of adaptive neuroplasticity following a peripheral vestibular lesion, which speaks for the robustness of [^{18}F]UCB-H PET as an imaging modality in brain plasticity research. Synaptic density imaging may be a more sensitive method to decipher subtle differences in peripheral deafferentation models with a comparable behavioral phenotype. In the future, [^{18}F]UCB-H PET may also be an interesting imaging modality to examine individual differences of central vestibular plasticity as a predictor of long-term outcomes in patients with acute vestibular disorders.

Funding

The current project was supported by funding from the German Ministry of Research and Education (BMBF 01 EO 1401) and funded by the European Union under Grant Agreement No 101120139.

Declaration of generative AI and AI-assisted technologies in the writing process

During the preparation of this work, the authors used ChatGPT (OpenAI) in order to check for grammar, spelling, and phrasing. After using this tool, the authors reviewed and edited the content as needed and take full responsibility for the content of the published article.

Data availability

The raw data supporting the conclusions of this article will be made available by the authors upon reasonable request, without undue reservation.

CRediT authorship contribution statement

Isabelle S. Fuxjäger: Writing – original draft, Visualization, Validation, Resources, Project administration, Methodology, Investigation, Formal analysis, Data curation, Conceptualization. **Melissa Antons:** Writing – review & editing, Validation, Resources, Methodology, Investigation. **Emna Marouane:** Writing – review & editing, Resources, Methodology, Conceptualization. **Giulia Leschiutta:** Writing – review & editing, Methodology, Investigation, Formal analysis. **Rosel Oos:** Writing – review & editing, Project administration, Methodology, Investigation. **Giovanna Palumbo:** Writing – review & editing, Project administration, Methodology, Investigation. **Dilara Steenken:** Writing – review & editing, Visualization, Methodology, Formal analysis, Data curation. **Simon Lindner:** Writing – review & editing, Resources, Project administration, Methodology, Investigation. **Sibylle Ziegler:** Writing – review & editing, Resources, Methodology, Formal analysis, Conceptualization. **Peter Bartenstein:** Writing – review & editing, Resources, Methodology, Conceptualization. **Matthias Brendel:** Writing – review & editing, Supervision, Resources, Project administration, Methodology, Formal analysis, Conceptualization. **Rudolf Werner:** Writing – review & editing, Supervision, Project administration, Methodology. **Andreas Zwergal:** Writing – original draft, Supervision, Resources, Project administration, Methodology, Investigation, Funding acquisition.

Declaration of competing interest

The authors report no conflicts of interest related to the current paper.

Acknowledgements

We thank Katie Göttlinger for copyediting the manuscript.

Supplementary materials

Supplementary material associated with this article can be found, in the online version, at doi:10.1016/j.neuroimage.2026.121821.

References

Antons, M., Lindner, M., Eilles, E., Günther, L., Delker, A., Branner, C., Krämer, A., Beck, R., Oos, R., Wuehr, M., Ziegler, S., Strupp, M., Zwergal, A., 2023. Dose- and application route-dependent effects of betahistine on behavioral recovery and neuroplasticity after acute unilateral labyrinthectomy in rats. Front. Neurol. 14, 1175481. https://doi.org/10.3389/fneur.2023.1175481.

Antons, M., Lindner, M., Grosch, M., Oos, R., Palumbo, G., Brendel, M., Ziegler, S., Bartenstein, P., Dieterich, M., Zwergal, A., 2022. Longitudinal (18)UCB-H/(18)FFDG imaging depicts complex patterns of structural and functional neuroplasticity following bilateral vestibular loss in the rat. Sci. Rep. 12, 6049. https://doi.org/10.1038/s41598-022-09936-w.

Beck, R., Günther, L., Xiong, G., Potschka, H., Böning, G., Bartenstein, P., Brandt, T., Jahn, K., Dieterich, M., Strupp, M., La Fougère, C., Zwergal, A., 2014. The mixed blessing of treating symptoms in acute vestibular failure — evidence from a 4-aminopyridine experiment. Exp. Neurol. 261, 638–645. https://doi.org/10.1016/j.expneurol.2014.08.013.

Bergquist, F., Ludwig, M., Dutia, M.B., 2008. Role of the commissural inhibitory system in vestibular compensation in the rat. J. Physiol. (Lond.) 586, 4441–4452. https://doi.org/10.1113/jphysiol.2008.155291.

Bertoglio, D., Halloin, N., Lombaerde, S.de, Jankovski, A., Verhaeghe, J., Nicaise, C., Staelens, S., 2022. SV2A PET imaging is a noninvasive marker for the detection of spinal damage in experimental models of spinal cord injury. J. Nucl. Med.: Official Publication, Soc. Nucl. Med. 63, 1245–1251. https://doi.org/10.2967/jnumed.121.263222.

Best, C., Lange, E., Buchholz, H.-G., Schreckenberger, M., Reuss, S., Dieterich, M., 2014. Left hemispheric dominance of vestibular processing indicates lateralization of cortical functions in rats. Brain Struct. Funct. 219, 2141–2158. https://doi.org/10.1007/s00429-013-0628-1.

Borghammer, P., Aanerud, J., Gjedde, A., 2009. Data-driven intensity normalization of PET group comparison studies is superior to global mean normalization. NeuroImage 46, 981–988. https://doi.org/10.1016/j.neuroimage.2009.03.021.

Carson, R.E., Naganawa, M., Toyonaga, T., Koohsari, S., Yang, Y., Chen, M.-K., Matuskey, D., Finnema, S.J., 2022. Imaging of synaptic density in neurodegenerative disorders. J. Nucl. Med.: Official Publication, Soc. Nucl. Med. 63, 60S–67S. https://doi.org/10.2967/jnumed.121.263201.

Conrad, J., Baier, B., Eberle, L., Ruehl, R.M., Boegle, R., Zwergal, A., Dieterich, M., 2023. Network architecture of verticality processing in the Human thalamus. Ann. Neurol. 94, 133–145. https://doi.org/10.1002/ana.26652.

Delva, A., van Laere, K., Vandenberghe, W., 2023. Longitudinal imaging of regional brain volumes, SV2A, and glucose metabolism In Huntington's Disease. Mov. Disord.: Official J. Movement Disord. Soc. 38, 1515–1526. https://doi.org/10.1002/mds.29501.

Dieterich, M., Bense, S., Lutz, S., Drzezga, A., Stephan, T., Bartenstein, P., Brandt, T., 2003. Dominance for vestibular cortical function in the non-dominant hemisphere. Cerebral Cortex 13, 994–1007. https://doi.org/10.1093/cercor/13.9.994 (New York, N.Y.: 1991).

Dutheil, S., Lacour, M., Tighilet, B., 2011. Neurogenic potential of the vestibular nuclei and behavioural recovery time course in the adult cat are governed by the nature of the vestibular damage. PLoS One 6, e22262. https://doi.org/10.1371/journal.pone.0022262.

Facchini, J., Rastoldo, G., Xerri, C., Péricat, D., El Ahmadi, A., Tighilet, B., Zennou-Azogui, Y., 2021. Unilateral vestibular neurectomy induces a remodeling of somatosensory cortical maps. Prog. Neurobiol. 205, 102119. https://doi.org/10.1016/j.pneurobio.2021.102119.

Grosch, M., Lindner, M., Bartenstein, P., Brandt, T., Dieterich, M., Ziegler, S., Zwergal, A., 2021. Dynamic whole-brain metabolic connectivity during vestibular compensation in the rat. NeuroImage 226, 117588. https://doi.org/10.1016/j.neuroimage.2020.117588.

Günther, L., Beck, R., Xiong, G., Potschka, H., Jahn, K., Bartenstein, P., Brandt, T., Dutia, M., Dieterich, M., Strupp, M., La Fougère, C., Zwergal, A., 2015. N-acetyl-L-leucine accelerates vestibular compensation after unilateral labyrinthectomy by action in the cerebellum and thalamus. PloS One 10, e0120891. https://doi.org/10.1371/journal.pone.0120891.

Hildebrandt, H., Hoffmann, N.A., Illing, R.-B., 2011. Synaptic reorganization in the adult rat's ventral cochlear nucleus following its total sensory deafferentation. PloS One 6, e23686. https://doi.org/10.1371/journal.pone.0023686.

Howes, O., Marcinkowska, J., Turkheimer, F.E., Carr, R., 2024. Synaptic changes in psychiatric and neurological disorders: state-of-the art of in vivo imaging. Neuropsychopharmacol.: Official Publication of the Am. College of Neuropsychopharmacol. 50, 164–183. https://doi.org/10.1038/s41386-024-01943-x.

Kaufman, G.D., Anderson, J.H., Beitz, A.J., 1993. Otolith-brain stem connectivity: evidence for differential neural activation by vestibular hair cells based on quantification of FOS expression in unilateral labyrinthectomized rats. J. Neurophysiol. 70, 117–127. https://doi.org/10.1152/jn.1993.70.1.117.

Lambert, F.M., Malinvaud, D., Gratacap, M., Straka, H., Vidal, P.-P., 2013. Restricted neural plasticity in vestibulospinal pathways after unilateral labyrinthectomy as the origin for scoliotic deformations. J. Neurosci.: Official J. Soc. Neurosci. 33, 6845–6856. https://doi.org/10.1523/JNEUROSCI.4842-12.2013.

Lindner, M., Gosewisch, A., Eilles, E., Branner, C., Krämer, A., Oos, R., Wolf, E., Ziegler, S., Bartenstein, P., Brandt, T., Dieterich, M., Zwergal, A., 2019. Ginkgo biloba extract EGb 761 improves vestibular compensation and modulates cerebral vestibular networks in the rat. Front. Neurol. 10, 147. https://doi.org/10.3389/fneur.2019.00147.

Marouane, E., Rastoldo, G., El Mahmoudi, N., Péricat, D., Chabbert, C., Artzner, V., Tighilet, B., 2020. Identification of new biomarkers of posturo-locomotor instability in a rodent model of vestibular pathology. Front. Neurol. 11.

Neuhauser, H.K., 2007. Epidemiology of vertigo. Curr. Opin. Neurol. 20, 40–46. https://doi.org/10.1097/WCO.0b013e328013f432.

Neuhauser, H.K., 2016. The epidemiology of dizziness and vertigo. Handb. Clin. Neurol. 137, 67–82. https://doi.org/10.1016/B978-0-444-63437-5.00005-4.

Péricat, D., Farina, A., Agavnian-Couquiaud, E., Chabbert, C., Tighilet, B., 2017. Complete and irreversible unilateral vestibular loss: a novel rat model of vestibular pathology. J. Neurosci. Methods 283, 83–91. https://doi.org/10.1016/j.jneumeth.2017.04.001.

Rastoldo, G., Marouane, E., El Mahmoudi, N., Péricat, D., Bourdet, A., Timon-David, E., Dumas, O., Chabbert, C., Tighilet, B., 2020. Quantitative evaluation of a new posturo-locomotor phenotype in a rodent model of acute unilateral vestibulopathy. Front. Neurol. 11.

Rastoldo, G., Marouane, E., El-Mahmoudi, N., Péricat, D., Watabe, I., Lapotre, A., Tonetto, A., López-Juárez, A., El-Ahmadi, A., Caron, P., Fraysse, M.-J.E., Chabbert, C., Zwergal, A., Tighilet, B., 2022. L-thyroxine improves vestibular compensation in a rat model of acute peripheral vestibulopathy: cellular and behavioral aspects. Cells 11. https://doi.org/10.3390/cells11040684.

Raymond, J., Ez-Zaher, L., Demêmes, D., Lacour, M., 1991. Quantification of synaptic density changes in the medial vestibular nucleus of the cat following vestibular neurectomy. Restor. Neurol. Neurosci. 3, 197–203. https://doi.org/10.3233/RNN-1991-3404.

Schiffer, W.K., Mirrione, M.M., Biegon, A., Alexoff, D.L., Patel, V., Dewey, S.L., 2006. Serial microPET measures of the metabolic reaction to a microdialysis probe implant. J. Neurosci. Methods 155, 272–284. https://doi.org/10.1016/j.jneumeth.2006.01.027.

Serrano, M.E., Bahri, M.A., Becker, G., Seret, A., Germonpré, C., Lemaire, C., Giacomelli, F., Mievis, F., Luxen, A., Salmon, E., Rogister, B., Raedt, R., Plenevaux, A., 2020. Exploring with (18)FUCB-H the in vivo variations in SV2A expression through the Kainic acid rat model of temporal lobe epilepsy. Molecular Imaging and Biol. 22, 1197–1207. https://doi.org/10.1007/s11307-020-01488-7.

Serrano, M.E., Becker, G., Bahri, M.A., Seret, A., Mestdagh, N., Mercier, J., Mievis, F., Giacomelli, F., Lemaire, C., Salmon, E., Luxen, A., Plenevaux, A., 2019. Evaluating the In vivo specificity of (18)FUCB-H for the SV2A protein, compared with SV2B and SV2C in rats using microPET. Molecules 24. https://doi.org/10.3390/molecules24091705.

Simon, F., Pericat, D., Djian, C., Fricker, D., Denoyelle, F., Beraneck, M., 2020. Surgical techniques and functional evaluation for vestibular lesions in the mouse: unilateral labyrinthectomy (UL) and unilateral vestibular neurectomy (UVN). J. Neurol. 267, 51–61. https://doi.org/10.1007/s00415-020-09960-8.

Strupp, M., Bisdorff, A., Furman, J., Hornibrook, J., Jahn, K., Maire, R., Newman-Toker, D., Magnusson, M., 2022. Acute unilateral vestibulopathy/vestibular neuritis: diagnostic criteria. J. Vestibular Res.: Equilibrium & Orientation 32, 389–406. https://doi.org/10.3233/VES-220201.

Tighilet, B., Manrique, C., Lacour, M., 2009. Stress axis plasticity during vestibular compensation in the adult cat. Neuroscience 160, 716–730.

Tighilet, B., Chabbert, C., 2019. Adult neurogenesis promotes balance recovery after vestibular loss. Prog. Neurobiol. 174, 28–35. https://doi.org/10.1016/j.pneurobio.2019.01.001.

Vignaux, G., Chabbert, C., Gaboyard-Niay, S., Travo, C., Machado, M.L., Denise, P., Comoz, F., Hitier, M., Landemore, G., Philoxène, B., Besnard, S., 2012. Evaluation of the chemical model of vestibular lesions induced by arsanilate in rats. Toxicol. Appl. Pharmacol. 258, 61–71. https://doi.org/10.1016/j.taap.2011.10.008.

Xiong, M., Roshanbin, S., Sehlin, D., Hansen, H.D., Knudsen, G.M., Rokka, J., Eriksson, J., Syvänen, S., 2023. Synaptic density in aging mice measured by [18F] SynVesT-1 PET. NeuroImage 277, 120230.

Zwergal, A., Dieterich, M., 2020. Vertigo and dizziness in the emergency room. Curr. Opin. Neurol. 33, 117–125. https://doi.org/10.1097/WCO.0000000000000769.

Zwergal, A., Günther, L., Brendel, M., Beck, R., Lindner, S., Xiong, G., Eilles, E., Unterrainer, M., Albert, N.L., Becker-Bense, S., Brandt, T., Ziegler, S., La Fougère, C., Dieterich, M., Bartenstein, P., 2017. In vivo imaging of glial activation after unilateral labyrinthectomy in the rat: a 18FGE180-PET study. Front. Neurol. 8, 665. https://doi.org/10.3389/fneur.2017.00665.

Zwergal, A., Lindner, M., Grosch, M., Dieterich, M., 2022. In vivo neuroplasticity in vestibular animal models. Mol. Cell. Neurosci. 120, 103721. https://doi.org/10.1016/j.mcn.2022.103721.

Zwergal, A., Schlichtiger, J., Xiong, G., Beck, R., Günther, L., Schniepp, R., Schöberl, F., Jahn, K., Brandt, T., Strupp, M., Bartenstein, P., Dieterich, M., Dutia, M.B., La Fougère, C., 2016. Sequential (18)FFDG μpet whole-brain imaging of central vestibular compensation: a model of deafferentation-induced brain plasticity. Brain Struct. Funct. 221, 159–170. https://doi.org/10.1007/s00429-014-0899-1.